Carbohydrate Polymers 118 (2015) 209–217

Contents lists available at ScienceDirect

Carbohydrate Polymers

journal homepage: www.elsevier.com/locate/carbpol

Theranostic magnetoliposomes coated by carboxymethyl dextran with controlled release by low-frequency alternating magnetic field

Hongyan Guo [1], Wansong Chen [1], Xiaoyi Sun, You-Nian Liu, Juan Li*, Jianxiu Wang*

College of Chemistry and Chemical Engineering, Central South University, 932 Lushan Road, Changsha 410083, Hunan, PR China

ARTICLE INFO

Article history:
Received 14 August 2014
Received in revised form 12 October 2014
Accepted 29 October 2014
Available online 25 November 2014

Keywords:
Liposome
Carboxymethyl dextran
Controlled release
Magnetic resonance imaging
Doxorubicin

ABSTRACT

The aim of this work was to construct carboxymethyl dextran (CMD)-coated magnetoliposomes (MLs), another stealth MLs alternative to PEGylated MLs, for theranostic application. Particularly, the on-demand release of CMD-MLs under low-frequency alternating magnetic field (LF-AMF) was studied. We found that as-prepared MLs exhibited good stability and high drug loading ability for doxorubicin (DOX). Cytotoxicity assay against human neuroblastoma SH-SY5Y cells showed that the DOX-loaded CMD-MLs were less toxic than free DOX due to the sustained release of DOX. However, the release of DOX-loaded CMD-MLs was enhanced by low-frequency alternating magnetic field without hyperthermia generation. The MLs also acted as an efficient T_2-weighted contrast agent during *in vitro* MRI measurements. The above results provide useful information on *in vivo* diagnostic/therapeutic efficacy of DOX-loaded CMD-MLs for some cancers, such as brain cancers.

1. Introduction

Theranostic nano-drug delivery systems (DDSs), which integrate imaging and therapeutic functions into a single platform for elaborating personalized therapeutic protocols to achieve the maximal benefit along with high safety, are attracting numerous attentions in treatment of cancer and other severe diseases (Mura & Couvreur, 2012). Magnetoliposomes (MLs), as the hybrids of magnetic components and phospholipid assemblies (Soenen, Vande Velde, Ketkar-Atre, Himmelreich, & De Cuyper, 2011), have being widely developed in theranostic applications. For example, MLs which encapsulate Fe_3O_4 nanoparticles could successfully act as a MRI-visible drug delivery system with targeting properties to both tumors and tumor microenvironment (Mikhaylov et al., 2011). However, controlled release and long-term stability are two key issues that should be addressed during the construction of MLs.

Controlled release of liposomes can be triggered by stimuli such as pH, temperature, redox, magnetic field and light, in order to improve the local drug bioavailability and to reduce the probability of drug resistance from low drug dosages at the targeted site (Chen et al., 2014; Preiss & Bothun, 2011; Wang, Chen, Yang, Yang, & Liu, 2014). Especially, externally on-demand release could be preferable for personalized medicine due to the high heterogeneity of tumor environments. Usually, controlled release for MLs can be also achieved by using magnetic hyperthermia-triggering approach on the thermosensitive components on the membrane (Katagiri et al., 2011; Tai et al., 2009), where high-frequency alternating magnetic field (in the range of hundreds of kilohertz or higher) is often applied. However, such a design may be not suitable for the cases where temperature changes are detrimental, such as in the brain tissues and highly perfused organs (kidney, liver, lung) (Jordan, Scholz, Wust, Fahling, & Felix, 1999). Hence, controlled release triggered by low-frequency alternating magnetic field (LF-AMF) would be highly desirable in which no hyperthermia was produced. For example, Nair et al. (2013) recently reported on-demand release of anti-HIV drugs using magneto-electric nanoparticles as carriers by applying LF-AMF, which could deliver anti-retroviral drugs across the blood-brain barrier. As well, controlled release of MLs under LF-AMF could be achieved (Nappini, Al Kayal, Berti, Norden, & Baglioni, 2011; Nappini, Bombelli, Bonini, Norden, & Baglioni, 2010; Spera et al., 2014).

Long-term stability of liposomes can be improved by outlayer coating of hydrophilic polymers, especially PEG (Smistad, Boyum, Alund, Samuelsen, & Hiorth, 2012). Nevertheless, PEGylation is prone to induce accelerated blood clearance (ABC) which limits its applications (Ishida et al., 2005; Shiraishi & Yokoyama, 2013). Carboxymethyl dextran (CMD), a kind of biodegradable and biocompatible anionic polymer, has been proved as low-fouling surface coatings and can be applied in blood substitutes (Chang, Crawford, & West, 1980), pro-drugs (Sugahara, Kajiki, Kuriyama, & Kobayashi, 2007) and biosensors (Lahiri, Isaacs, Tien, & Whitesides,

* Corresponding authors. Tel.: +86 73188836964.
E-mail addresses: juanli@csu.edu.cn (J. Li), jxiuwang@csu.edu.cn (J. Wang).
[1] Guo H. and Chen W. contributed equally.

http://dx.doi.org/10.1016/j.carbpol.2014.10.076
0144-8617/

1999). Typically, superparamagnetic nanoparticles coated with carboxydextran can now be used as MRI agents (commercially Resovist®) (Lunov et al., 2010). Earlier studies showed that the external magnetic field could enhance the aggregation of CMD-coated magnetic nanoparticles (MNPs) in the rat brain (Huang et al., 2009). We previously synthesized CMD-coated liposomes (CMD-LIPs) and found that the DOX-loaded CMD-LIPs were stable and could effectively prevent aggregation under physiological buffers and serum media (Ning et al., 2011). In this work, we attempted to construct stealth CMD-MLs, alternative to PEGylated MLs, for theranostic application. Particularly, this work aimed to study the controlled release of CMD-MLs under LF-AMF to avoid hyperthermia generation for the potential application for some cancers, such as brain cancers. The physicochemical properties, morphology, MRI performance and cytotoxicity of CMD-MLs were examined *in vitro*. Their drug loading and release behaviors were also assessed in which DOX was used as an anticancer drug model.

2. Experimental

2.1. Materials

Soybean phosphatidylcholine (Lipoid S 100) was purchased from Toshisun Lipoid (Shanghai, China). Doxorubicin hydrochloride (DOX, 98%) was obtained from Huafeng Co. Ltd. (Beijing, China). Dextran T-10 was purchased from Pharmacia (Uppsala, Sweden). Iron(III) chloride ($FeCl_3$), iron(II) chloride ($FeCl_2$), tri-sodium citrate, perchloric acid and cholesterol, were purchased from Sigma-Aldrich (St. Louis, MO). All aqueous solutions were prepared using Millipore water (18 MΩ cm, Simplicity Model, Billerica, MA). Other commonly used reagents and solvents were of analytical purity and used without further purification. SH-SY5Y cells were obtained from the Xiangya Hospital of Central South University (Changsha, China).

2.2. Synthesis of amphiphilic CMD

Amphiphilic CMD was synthesized according to our published procedure (Ning et al., 2011). Briefly, CMD was first synthesized by reaction of dextran with bromoacetic acid in alkali solution. Afterwards, oleylamine was conjugated to CMD in the presence of the coupling agents NHS/EDC. The contents of carboxyl groups of amphiphilic CMD were determined by titration. The degree of carboxymethylation was about 21% and the degree of amidation was about 6%.

2.3. Synthesis of superparamagnetic iron oxide nanoparticles (SPIONs)

SPIONs were prepared by modified chemical co-precipitation method with two-step surface tailoring procedure according to the Massart's (1981) procedure. Specifically, the method was firstly modified by perchloric acid-etching for positive surface and then by citrate-coating for negative surface. Briefly, an aqueous mixture of $FeCl_3$ (40 mL, 1 M) and $FeCl_2$ (10 mL, 2 M) was added to ammonia solution (250 mL, 0.7 M). Then the pH was adjusted to 10–11 with ammonia solution. The gelatinous precipitate was stirred for 30 min before being isolated from the solution by magnetic decantation. Further, the precipitate was stirred with perchloric acid (100 mL, 2 M) solution for 30 min and then was isolated by magnetic decantation. Following this, for negative SPIONs, the precipitate was incubated with tri-sodium citrate (50 mL, 0.25 g L^{-1}) solution for 30 min. After magnetic decantation, the black precipitate was washed twice with water. Black powder of SPIONs was obtained after lyophilization.

2.4. Preparation of the CMD-MLs and DOX-loaded CMD-MLs

CMD-MLs, i.e., SPIONs-encapsulated CMD-coated liposomes were prepared by thin-lipid film hydration method. Briefly, the lipid compositions for MLs are as follows: phosphatidylcholine:cholesterol:amphiphilic CMD = 55:40:0.5 (molar ratio). Lipid components (100 mg) were dissolved in 4 mL of chloroform/methanol mixture (3/1, v/v), then the solution was dried to a thin lipid film under vacuum. The lipid film was hydrated with 10 mL of mixture solution of SPIONs (5 mg) and ammonium sulfate (330 mg) in water, then the colloidal solution was sonicated for 30 min. The liposomal solution was centrifuged at 14,000 rpm for 5 min to remove the unencapsulated SPIONs. Under the centrifuge, unencapsulated SPIONs remained suspended as checked by DLS. Abandoning the supernatant, the precipitate was dispersed in 250 mM ammonium sulfate again, and finally the CMD-MLs were obtained.

DOX was remotely loaded into the MLs by ammonium sulfate gradient. First, 10 mL of empty liposomal solution (10 mg mL^{-1}) was formed in 250 mM ammonium sulfate solution as described above. Then, free ammonium sulfate solution was removed by dialysis against PBS (pH 7.4, 0.01 M). After dialysis, the solution was transferred into a flask and incubated at 45 °C for 1 h, followed by the addition of DOX (20 mg). DOX-loaded MLs were obtained after overnight incubation at 45 °C, and then dialyzed against deionized water to remove the unloaded DOX. The DOX-loaded MLs were stored at 4 °C before use.

Control liposomes, such as uncoated liposomes (UC-LIPs), uncoated MLs (UC-MLs), CMD-coated liposomes (CMD-LIPs) were prepared using the same procedure as CMD-MLs, except the absence of SPIONs and/or amphiphilic CMD.

2.5. Encapsulation efficiency

Fe_3O_4 content was calculated by thermal gravimetric analysis (TGA, METTLER TGA/SDTA851e ThermoGravimetric Analyzer). The iron content in the CMD-MLs solution was determined by inductively coupled plasma-atomic emission spectrometry (ICP-AES 5300dv). DOX encapsulation efficiency of the MLs was calculated according to our previously reported method (Chen et al., 2014). The amount of DOX within the MLs was determined by UV–Vis absorbance at 490 nm (SHIMADZU, UV-2450) after destroying the MLs within 0.1% Triton X-100 solution.

2.6. Generation of LF-AMF

The apparatus for generation of LF-AMF was assembled as described in Supplementary data (Fig. S1). Briefly, an adjustable magnetic field was generated by a solenoid of 1.1×10^4 turns per meter through which an alternating electric current (50 Hz) was led. The length of the solenoid was 28 cm. A resistance box was used to minimize the self-inductance. Samples were placed in the middle of the solenoid.

2.7. Dynamic light scattering (DLS) and ζ-potential measurements

The size distribution and ζ-potentials of the samples was carried out on a Malvern Zetasizer Nano ZS equipped with a 4 mW He–Ne laser 633 nm using the technique of laser doppler electrophoresis. The measurements were performed at 25 °C and a fixed scattering angle of 173°. Each sample was analyzed three times.

2.8. X-ray diffraction

X-ray diffraction (XRD) patterns of the powder after lyophilization were recorded with a D/max2550VB diffractometer equipped with source Cu $K\alpha$ radiation (λ = 0.15406 nm) at the step size 0.02° from 10° to 80° and the working voltage is 40 kV with 250 mA working current.

2.9. Atomic force microscopy (AFM)

The morphologies of the MLs were characterized by AFM (Veeco, NanoMan VS). AFM samples were prepared by the following procedures: freshly liposomal suspension was diluted to 100 μg mL^{-1} with deionized water, then deposited on freshly cleaved mica and dried in a desiccator containing dried silica gel for 72 h.

2.10. Vibrating sample magnetometer

Superparamagnetic properties of the samples were investigated at 300 K with an ADS DMS EV7 vibrating sample magnetometer with the applied magnetic field of ±4000 G.

2.11. MRI and relaxivity performance

The MRI performance of SPIONs and MLs was tested using a Siemens MRI scanner system with the magnetic field of 1.5 T, and the longitudinal and transverse relaxivities were measured using a MicoMR Analyzing system (Shanghai Niumag Corporation) with the magnetic field of 0.5 T. The relaxivity values, r_1 and r_2, were evaluated *via* the linear fitting of $1/T_2$ relaxation time (s^{-1}) *versus* the iron concentration (mM Fe), respectively.

2.12. Alternating magnetic field-induced release

In vitro release of DOX from the CMD-MLs was measured using a dialysis method (cut-off molecular weight of 3500 Da). Before dialysis, the samples were subjected under a LF-AMF (50 Hz) with certain magnetic field intensity for different exposure time. Then a solution of 0.5 mL DOX-loaded liposomes (1 mg mL^{-1} DOX) was transferred into a dialysis bag and dialyzed against 500 mL release medium (0.01 M PBS at pH 7.4 and 5.0). Then the release medium was stirred at 100 rpm at 37 °C. At the given sampling time, 2 mL of the medium were removed and replenished with 2 mL of fresh buffer. Throughout the experiment, the samples were protected from light. The concentration of released DOX was determined by fluorescent spectroscopy (F-4600) using an emission wavelength of 598 nm and an excitation wavelength of 490 nm. The error bars were obtained from triplicate samples.

2.13. Cell cytotoxicity

The cell cytotoxicities of DOX-loaded CMD-MLs were evaluated against SH-SY5Y cancer cell lines by the 3-(4,5-dimethylthiazol-2-yl)-2,5-diphenyltetrazolium bromide (MTT) assay. The cells were seeded in 96-well plates at a density of 1×10^4 cells per milliliter, cultured in DMEM/F-12 medium with 10% fetal bovine serum, 1% penicillin and 1% streptomycin, and kept in humidified environment at 37 °C containing 5% CO_2. After the cells anchored to the wells, they were treated with fresh culture solution with CMD-MLs and DOX-loaded CMD-MLs (serials of concentration: 0.1, 1.0, 2.5, 5.0, and 10 μg mL^{-1}) and incubated for 24 h, respectively. After incubation, 100 μL of MTT solution (final concentration 0.5 mg mL^{-1}) was added to each well and incubated for another 4 h. The MTT-formazan crystals formed by metabolically viable cells were dissolved in 100 μL DMSO. Finally, the absorbance was monitored by a microplate reader (Bio-Tek ELx800) at the wavelength of 490 nm. The cell viability is expressed as follows: Cell viability (%) = $A_T/A_0 \times 100$; where A_T is the absorbance of treated cells and A_0 is the control absorbance. Data of cell viability are given as mean ± standard deviation (S.D.).

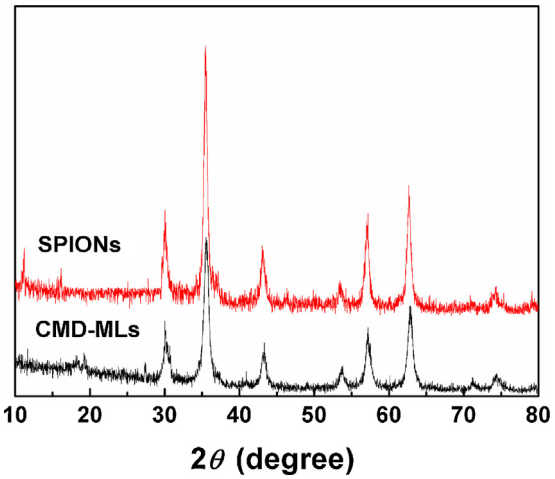

Fig. 1. XRD of SPIONs and CMD-MLs.

3. Results and discussion

3.1. Synthesis and characterization of SPIONs

In order to fabricate well dispersed CMD-MLs, the surface of SPIONs should be carefully designed. Based on the chemical co-precipitation method by Massart (1981), we used the two-step tailoring procedure (firstly perchloric acid-etching followed by citrate-coating). Briefly, the SPIONs were first etched for positive charges in the presence of perchloric acid, and then alternately coated by sodium citrate for negative charges.

The SPIONs treated by the two-step surface tailoring method are quite stable and well dispersed in aqueous solution. The size of the SPIONs, determined by TEM, is very small, about 3–5 nm in diameter (Fig. S2). However, the hydrodynamic diameter (D_h) based on DLS studies is about 35 nm. The XRD showed typical characteristic peaks of magnetite (Fe_3O_4) (Fig. 1), being in agreement with those reported (Casula et al., 2010). The SPIONs are superparamagnetic without the hysteresis in the magnetic profile (Fig. 2). The saturation magnetization (M_s) of SPIONs was found to be 61.4 emu/g, being less than that of the bulk (118.4 emu/g) (Lai et al., 2012), which might be mainly caused by the size and surface effect.

In addition, we found the SPIONs prepared by individual tailoring step method, *i.e.* citrate-coating or perchloric acid-etching method, was incapable of producing stable and well-dispersed magnetoliposomes. For instance, the SPIONs by the citrate-coating method, formed polydispersed particles, while the positive SPIONs by perchloric acid-etching produced large aggregates upon mixing with the negative CMD components.

3.2. Synthesis and physicochemical properties of CMD-MLs

In nanomedicine, it was established that the surface properties would affect their pharmacokinetic behaviors in variedly different ways. For example, the clearance rate of dextran-coated liposomes is dependent on the density of dextran molecules on the liposome surface (Pain, Das, Ghosh, & Bachhawat, 1984). The intracellular uptake of carboxydextran-coated SPIONs is dependent on the charged groups and on the type of target cell (Mailander et al., 2008). The purpose of this work is to find the optimal coating

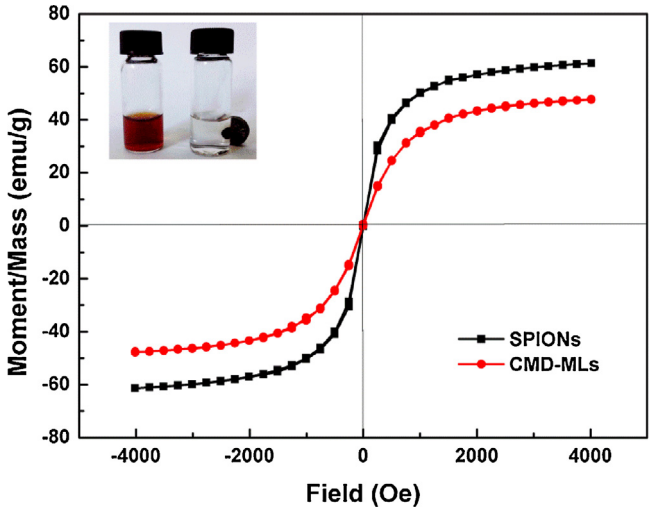

Fig. 2. Magnetization curves of SPIONs and CMD-MLs measured at 300 K. Inset: Images of magnetoliposomes before (left) and after (right) magnetic separation by a 0.3-T magnet.

material alternative to PEG, which could provide MLs stability in blood circulation, as discussed in the following text (Section 3.4).

In this study, we chose dextran T-10 as the precursor for the synthesis of CMD, followed by our previous study which has demonstrated liposomes coated by CMD have excellent stabilities in serum and property of preventing nonspecific protein adsorption (Ning et al., 2011). Dextran T-10 with a molecular weight of about 10 kDa, is one kind of polysaccharides, composed of 95% α-(1 → 6)-D-glucan linkages in the main chain and 5% other linkages in the branch when produced by *Leuconostoc mesenteroides* (Kitaoka & Robyt, 1999). This kind of dextran is water-soluble, facile for functionalization, and widely used for medical applications. For example, it was applied for the coating in the commercial superparamagnetic agents Endorem® (Lawaczeck et al., 1997).

CMD-MLs were prepared by the thin-lipid film hydration method, similar to our previous work (Ning et al., 2011). As shown in Scheme 1, SPIONs were encapsulated into the liposomes during the film hydration process. CMD-MLs possess much larger D_h than SPIONs, but still display unimodal size distribution around 120 nm (Fig. S3), indicating that most of the hydrophilic SPIONs are encapsulated into the liposomal cores. The size distribution of CMD-MLs is comparable to that of UC-LIPs, CMD-LIPs and UC-MLs (Table 1), which suggests that SPIONs have good stability and do not perturb the assembly of the lipid components. CMD-MLs have similar XRD pattern as SPIONs (Fig. 1), indicating that the SPIONs inside the CMD-MLs preserve their original crystalline structure. The slight difference in the low-intensity peaks for the CMD-MLs is due to the presence of coating layers on the surface of the SPIONs. The similar phenomenon was also observed for the starch-coated SPIONs (Gomes et al., 2009). The TGA measurement indicates that the content of Fe_3O_4 in the CMD-MLs was 6%, while that in the SPIONs was 83%. The content of Fe_3O_4 after encapsulation is a bit higher than that in the initial feed (5%), probably caused by the loss of lipid content during the centrifugation. The final iron content in the CMD-MLs suspension, assayed by atomic absorption spectrum, was about 2 mM.

The CMD-MLs exhibit similar superparamagnetic behavior as the SPIONs although the magnetic hysteresis loops of the MLs and SPIONs are different (Fig. 2). The M_s of the CMD-MLs was estimated to be 47.7 emu/g, being smaller than that of the SPIONs. Nevertheless, complete magnetic separation was achieved under a 0.3-T rare-earth magnet while examining the magnetic responsiveness of the CMD-MLs (inset in Fig. 2). These features are indicative of magnetic targeting in the applications of the CMD-MLs.

3.3. Morphology of CMD-MLs

AFM observed spherical particles of both SPIONs and CMD-MLs spread on the mica surface with the size of the SPIONs being much smaller than that of the CMD-MLs (Fig. 3). The increase in the height of the CMD-MLs (50–100 nm) in comparison with that of the SPIONs (10–20 nm) confirms that the SPIONs were encapsulated into the inner liposomal cores. The height of the CMD-MLs by AFM was smaller than the D_h by DLS, indicating that the liposomes were adhered to the mica surface after the drying process (Teschke & de Souza, 2002). Interestingly, the well-ordered MLs were found to be highly aligned on the matrix surface. Based on the previous reported work that the horizontal alignment of the peptide assemblies could be achieved *via* combination with iron nanoparticles under external magnetic field (Bolisetty, Vallooran, Adamcik, & Mezzenga, 2013; Reches & Gazit, 2006), our AFM results provide evidence that the liposomes are highly magnetic-responsive due to the encapsulation of the SPIONs though the unknown source of the magnetic field. Additionally, TEM was also used for the observation of CMD-MLs. The SPIONs were clearly seen inside the liposomes (Fig. S4).

3.4. Stability of SPIONs and CMD-MLs in serum

Broad size distribution of the SPIONs in the serum suggests that their stability was strongly affected (Fig. 4A). Whereas, evidenced by the unchanged size distribution (Fig. 4B), the CMD-MLs preserved good stability in the serum. The excellent stability of the CMD-MLs could be ascribed to the CMD coating and liposomal encapsulation. Previously the CMD-LIPs were found to have better stability than the uncoated liposomes in serum and display excellent active targeting properties after ligand coupling (Ning et al., 2011). PEGylation is generally regarded as the common approach used to enhance the stability of liposome during blood circulation, on the other hand, ABC phenomenon is also a well-known immunological response of PEG-coated liposomes and greatly influences targeting properties of delivery systems (Shiraishi & Yokoyama, 2013). Thus, alternatives to PEGylation are desirable. In this work, after incorporation of SPIONs, the CMD-MLs exhibit remarkable stability and good magnetic-responsive properties, providing an alternative platform to PEGylated MLs with enhanced targeting properties (passively and magnetically) in the systemic administration.

3.5. MRI performance of CMD-MLs

To examine the relaxivity of the MLs, longitudinal (T_1) and transverse proton relaxation times (T_2) were first measured as a function of ferric ion concentration. The relaxivity values of r_1 and r_2 were then determined to be 0.6 and 36 s^{-1} mM^{-1} based on the slopes of the linear plots of $1/T_1$ vs. iron concentration, and $1/T_2$ vs. iron concentration, respectively (Fig. 5 and Fig. S5). Generally, r_2 is a measure for the potential of T_2-weighted contrast agent. The r_2 of CMD-MLs is relatively lower than those of the commercial T_2-weighted contrast agent (about 164 s^{-1} mM for Resovist®) (Lawaczeck et al., 1997), magnetite-loaded liposome (in the range of 573–1286 s^{-1} mM^{-1}) (Mikhaylov et al., 2011) and magnetic nanoclusters with hydrophilic spacing (up to 604 s^{-1} mM) (Pothayee et al., 2013). Nevertheless, the ratio of r_2 to r_1, is also capable of measuring the potential of MLs as a contrast agent. When r_2/r_1 is greater than 10, the contrast agents are regarded as T_2-weighted contrast agents. The higher the r_2/r_1 value, the better the T_2-weighted contrast agent (Hao et al., 2013). The r_2/r_1 value of the CMD-MLs (value

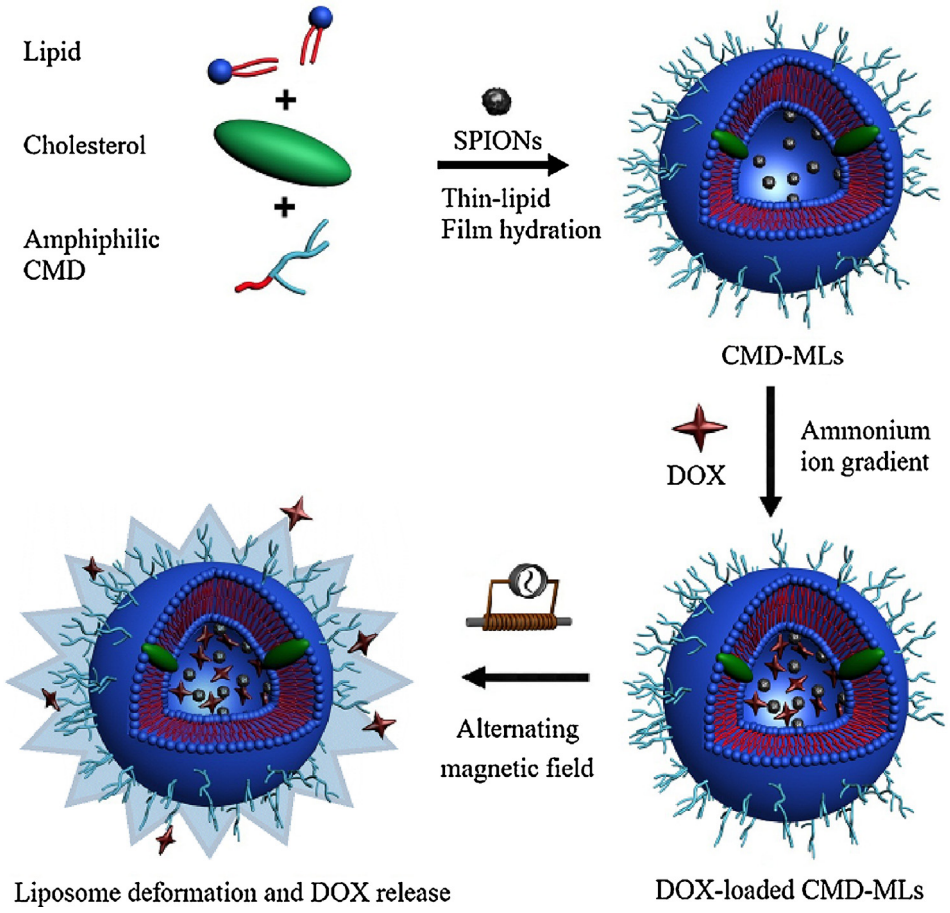

Scheme 1. Diagram of SPIONs-encapsulated and DOX-loaded CMD-MLs and the subsequent DOX release under LF-AMF.

of 57) is larger than that of the commercial Resovist (value of 7–17) (Liao et al., 2011; Mikhaylov et al., 2011), and is comparable to those of ultra magnetic liposomes (Bealle et al., 2012), indicating that the CMD-MLs could serve as a good candidate for T_2-weighted contrast agent. Note that r_1 reflects the spin-lattice relaxation process and generally decreases when water accessibility to MNPs is limited, while r_2 is related to the spin-spin relaxation process and usually increases for bigger nanoparticles (Martina et al., 2005; Thorek & Tsourkas, 2008). The reason for the lower r_2 but higher r_2/r_1 of the CMD-MLs remains unclear, where varied factors such as stability of the CMD-MLs, surface property of the SPIONs, and local concentration and clustering effect of iron nanoparticles account for it. Furthermore, T_2-weighted MR images of CMD-MLs with various iron concentrations were obtained (inset in Fig. 5). With iron concentration increase, the MR signal intensity of the MLs decreases dramatically for T_2-weighted pattern. These results together indicate that the MLs behave as an efficient T_2-weighted contrast agent for MRI.

3.6. DOX loading

One of the advantages for liposomal carriers is that their inner aqueous core can encapsulate a large amount of cargo molecules. To verify the effectiveness of the CMD-MLs as a good drug reservoir, traditional remote loading method was used to drive DOX into the CMD-MLs. Compared with uncoated liposomal systems (UC-LIPs and UC-MLs), the CMD-MLs displayed better DOX encapsulation efficiency (Table 1). In addition, the difference of drug loading ability between the CMD-LIPs and CMD-MLs was no significant since the loading space for DOX was not apparently occupied by the low content of the incorporated SPIONs. As for the encapsulation efficiency, competitive or synergetic effect of dual loading

Table 1
Physicochemical data of SPIONs and liposomal nanoparticles[a].

Samples	D_h (nm)	PDI	ζ-Potential (mV)	Encapsulation efficiency (%)
Fe_3O_4	35 ± 3	0.16 ± 0.03	−30.5 ± 0.4	N.A.[b]
UC-LIPs	91 ± 8	0.13 ± 0.02	−7.8 ± 0.5	N.A.
CMD-LIPs	111 ± 4	0.18 ± 0.01	−29.8 ± 0.3	N.A.
UC-MLs	112 ± 11	0.21 ± 0.06	−27.8 ± 1.3	N.A.
CMD-MLs	120 ± 6	0.17 ± 0.01	−24.9 ± 0.4	N.A.
DOX-UC-LIPs	149 ± 7	0.23 ± 0.04	5.4 ± 0.3	84.1 ± 0.6
DOX-CMD-LIPs	169 ± 3	0.15 ± 0.02	5.6 ± 0.7	98.4 ± 0.4
DOX-UC-MLs	193 ± 12	0.22 ± 0.06	−26.1 ± 0.7	80.9 ± 0.3
DOX-CMD-MLs	220 ± 8	0.13 ± 0.03	−24.9 ± 0.4	96.9 ± 0.6

[a] The standard deviation (S.D.) was obtained from at least three replicate measurements.
[b] Not applicable.

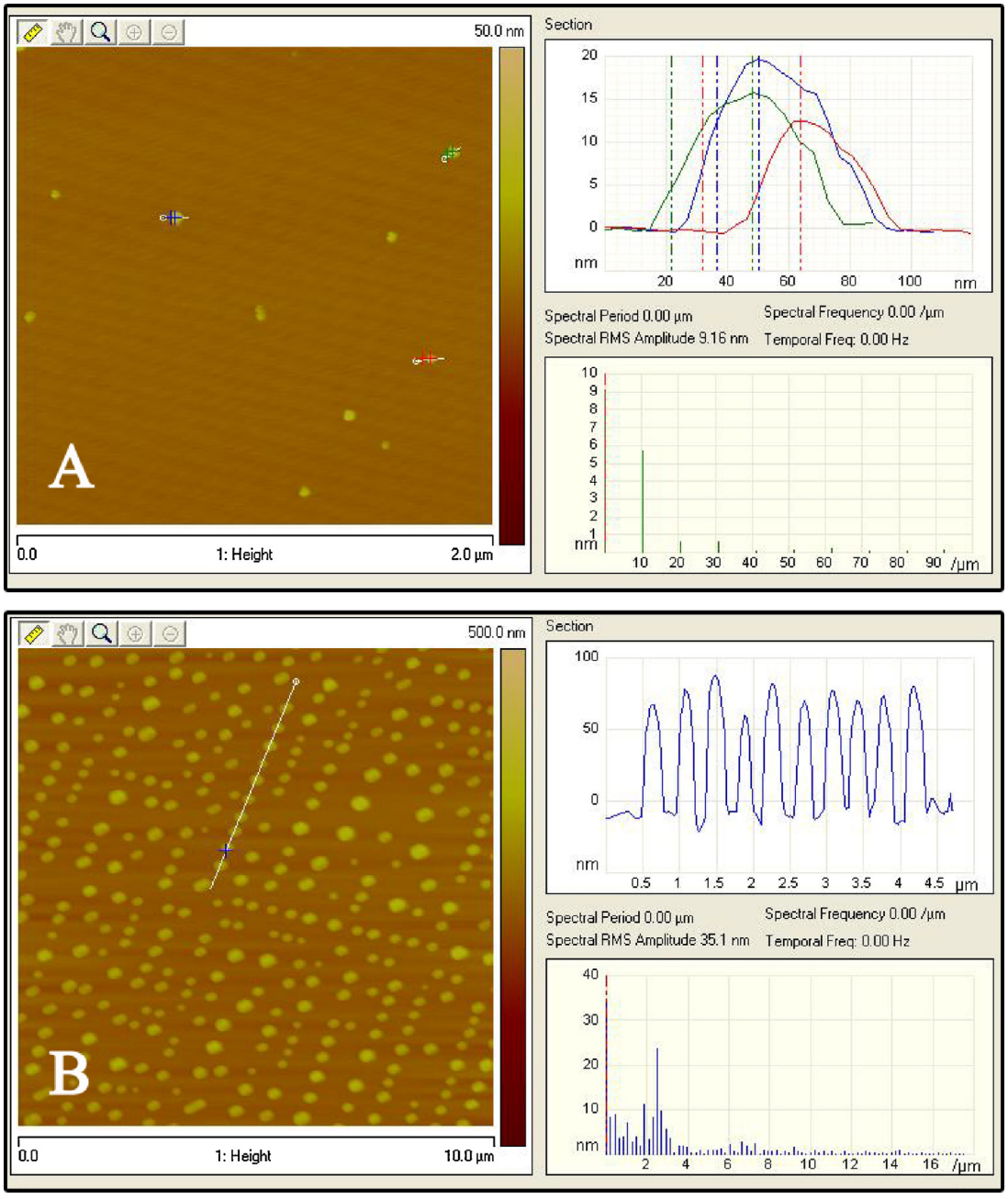

Fig. 3. AFM images of SPIONs (A) and CMD-MLs (B).

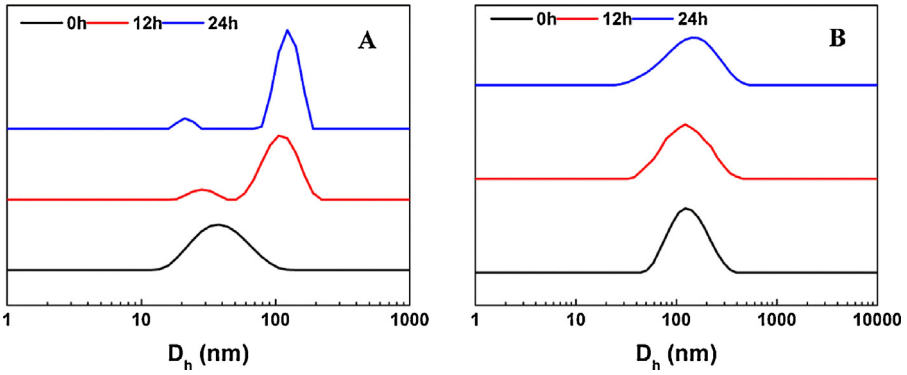

Fig. 4. Size distribution of SPIONs (A) and CMD-MLs (B) measured by DLS before and after incubation in calf serum.

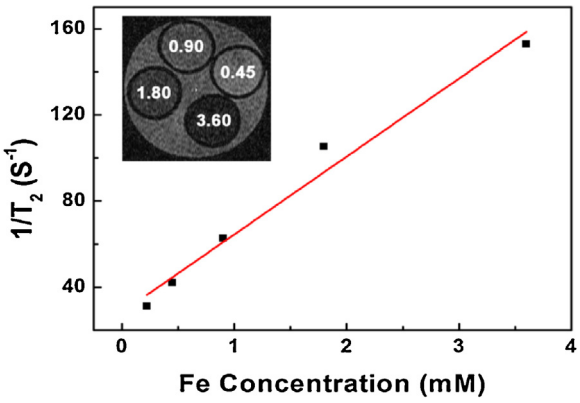

Fig. 5. Inversed relaxation time ($1/T_2$) as a function of Fe concentration under a 0.5-T magnetic field. Inset: T_2-weighted imaging of MLs suspension serially diluted to various Fe concentrations.

or co-encapsulation depending on the structure features has been observed for polymersomes. For example, the DOX encapsulation efficiency was decreased by 22% when 35 wt% hydrophobic MNPs were loaded in block copolymer vesicles (Sanson et al., 2011), the encapsulation efficiency in the folate-targeted DOX-containing MLs (MagFolDox) was about 85% and 24% for DOX and MNPs, respectively (Pradhan et al., 2010). Also, we found that the size of DOX-loaded CMD-MLs became somewhat larger after DOX loading. However, such a size (merely about 220 nm) is still suitable for the EPR effect. Hence, dual loading of DOX and MNPs into the liposomal carriers was performed in the present work.

3.7. DOX release under LF-AMF

The effect of LF-AMF on the release of DOX from DOX-loaded CMD-MLs was monitored under different magnetic field intensities (15, 30 and 50 mT) and different time courses (10, 20 and 30 min). As the extracellular pH of tumors is slightly acidic than that of blood and normal tissues, we examined the drug release in buffers of pH 5.0 and 7.4. Fig. 6 shows the release patterns of the CMD-MLs were greatly altered after exposure to LF-AMF. Initial rapid release was followed by a slower process and much more cumulative release of DOX was obtained when CMD-MLs underwent exposure time. By contrast, in the absence of LF-AMF, little initial release was observed for the CMD-MLs and the cumulative release was much less. For example, after exposure to 45 mT-LF-AMF for 30 min, 74% of DOX release was achieved at pH 5.0, while only 35% was obtained in the absence of LF-AMF during the first 24 h-incubation at pH 5.0.

We also found the release of the CMD-MLs was faster at pH 5.0 than at pH 7.4 in the absence/presence of LF-AMF, due to the pH-sensitive stability of CMD-MLs. In the absence of LF-AMF, the minimum release (<30%) of DOX was achieved after incubation at pH 7.4 for 72 h (Fig. 6B and D). After exposure to LF-AMF, the CMD-MLs still exhibited a slower release rate at pH 7.4 than that at pH 5.0. As a control, the effect of magnetic field on the release of DOX-loaded CMD-LIPs without SPIONs incorporation was negligible (data not shown).

To understand the influence of LF-AMF on the structure of CMD-MLs, the size distribution of the CMD-MLs after LF-AMF treatment was checked by DLS. The D_h and PDI (458 nm and 0.58, respectively) of the CMD-MLs became much larger after exposure to the LF-AMF at pH 5.0. Meanwhile, the encapsulation efficiency was decreased to 76.8% after exposure to 30 mT-LF-AMF for 30 min. Thus, the initial release of the CMD-MLs under LF-AMF was attributed to the drug leakage resulting from the structure deformation of liposomes. As several studies investigated, LF-AMF can influence the drug release of MLs through alteration the lipid permeability without the collapse of the lipid membrane (Nappini et al., 2010, 2011). The reason for the significant change in size of CMD-MLs could be ascribed to the coating by the pH-sensitive CMD. Furthermore, no apparent bulk heat was measured in the bulk solution after the CMD-MLs

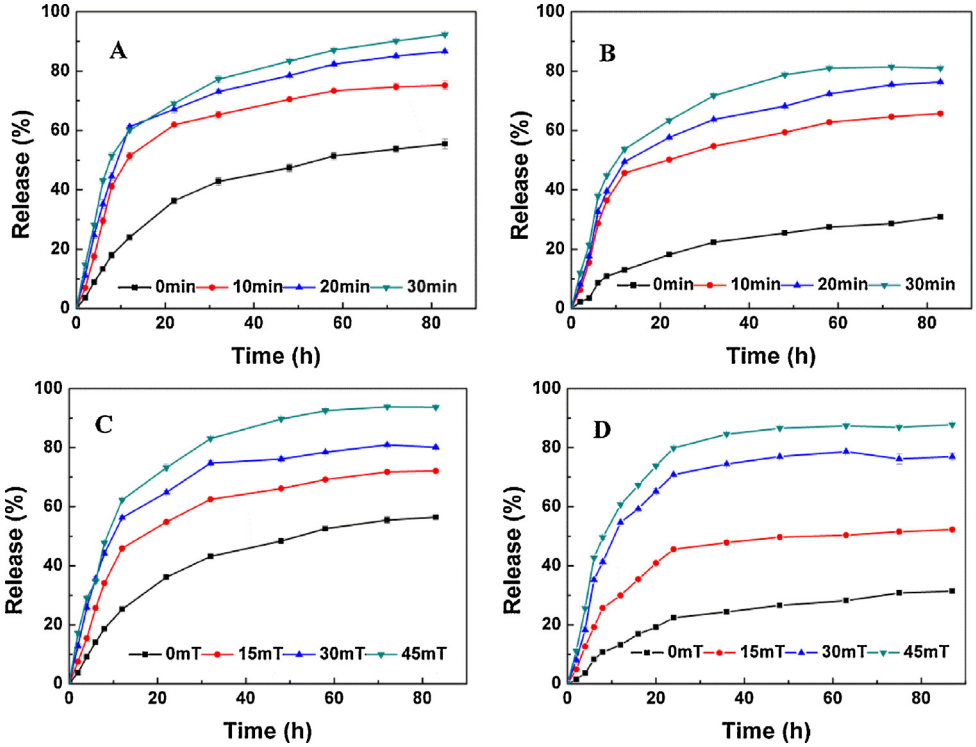

Fig. 6. Release of DOX from CMD-MLs under pH 5.0 (A) and pH 7.4 (B) after exposure to LF-AMF (50 Hz, 30 mT) under different time courses, and release of DOX from CMD-MLs under pH 5.0 (C) and pH 7.4 (D) after exposure to LF-AMF of various intensities for 10 min.

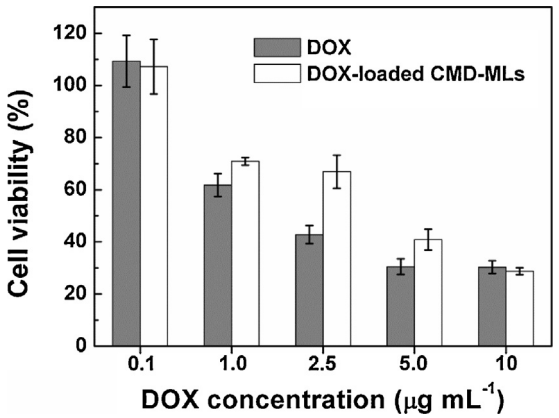

Fig. 7. Cytotoxicity of DOX-loaded CMD-MLs against SH-SY5Y cells at various DOX concentrations after 24 h-incubation. Error bars mean S.D. ($n = 3$).

were exposed to the LF-AMF. Our results are consistent with the major feature of controlled release by LF-AMF without hyperthermia generation (Nappini et al., 2010).

3.8. Cytotoxicity

As mentioned above, the LF-AMF-triggered drug release system exhibits certain advantages over the high-frequency AMF one due to the hyperthermia effect of the latter one, which is not suitable for the tissues (*e.g.* brain) that are susceptible to environmental temperature change (Nair et al., 2013; Tai et al., 2009). DOX has been used to treat the brain cancer (Belloni, Uberti, Rizzini, Jiricny, & Memo, 1999), however, our DOX-loaded CMD-MLs in the absence of magnetic actuation have a sustained-release pattern, which would compromise the drug potent in cancer treatment by decreasing the low drug bioavailability and increasing the probability of drug resistance. To verify the necessity of magnetically triggered release to enhance the therapeutic efficacy *in vivo*, the cytotoxicities of free DOX and DOX-loaded CMD-MLs against the human neuroblastoma SH-SY5Y cells were compared. As shown in Fig. 7, the viability of SH-SY5Y cells after incubation with DOX-loaded CMD-MLs for 24 h was higher than that treated by free drugs at concentrations of 1.0, 2.5, 5.0 μg/mL. Note that the unloaded CMD-MLs exhibited little cytotoxicity (data not shown). DOX-loaded CMD-MLs display similar lower cytotoxicity results than free DOX as other DOX liposomal formulation do in the absence of LF-AMF (Goren et al., 2000; Xiong et al., 2005) The lower cytotoxicity of DOX-loaded MLs could be ascribed to the low drug availability from sustained release of DOX or lower cellular uptake than free DOX.

DOX exerts anticancer activity by intercalating with the double-stranded helix DNA in nuclei after internalization, so intracellular DOX delivery is essential to its anticancer activity (Goren et al., 2000; Xiong et al., 2005). As for free DOX, the cytotoxicity is high because free DOX enters the cells by diffusion. By contrast, the DOX liposomal formulation is less cytotoxic because the internalization of liposomal DOX is limited by membrane diffusion and sustained release, and might be enhanced through cell uptake and/or triggering release process. Thus, it would be helpful to trigger the drug release from the liposomes by LF-AMF after they are magnetically-guided into the target sites. Further *in vivo* animal study is now being carried out in our lab to validate the application.

4. Conclusions

Carboxymethyl dextran-coated magnetoliposomes (CMD-MLs) have been successfully fabricated, where the key process involved a two-step surface tailoring procedure of the precursor SPIONs. The as-prepared CMD-MLs displayed narrow size distribution, superparamagnetic property, and high stability in serum. The dual loading of DOX and MNPs was examined and the release process was pH- and magnetic- dependent. Notably, the DOX release was greatly promoted by the LF-AMF. CMD-MLs also acted as an efficient T_2-weighted contrast agent during *in vitro* MRI measurements. The CMD-MLs described herein thus are capable of serving as a potential carrier for targeting diagnostic-therapy for some cancers, such as brain cancers. The drug release could be modulated by LF-AMF after drugs are magnetically guided and/or passively targeted to the pathological tissues, without generation of hyperthermia effect on the neighboring healthy tissues.

Acknowledgments

This work was supported by the National Natural Science Foundation of China (nos. 21374133, 21276285 and 21104096) and Hunan Provincial Natural Science Foundation of China (No. 12JJ4014). The authors express grateful thanks to Mr. Yanqun Liu (School of Physics and Electronics, Central South University, China) for the help of assembling the apparatus of AMF. We also owed our thanks to Prof. Aiguo Wu (Ningbo Institute of Materials Technology and Engineering, Chinese Academy of Sciences, China) for his help in MRI.

Appendix A. Supplementary data

Supplementary data associated with this article can be found, in the online version, at http://dx.doi.org/10.1016/j.carbpol.2014.10.076.

References

Bealle, G., Di Corato, R., Kolosnjaj-Tabi, J., Dupuis, V., Clement, O., Gazeau, F., et al. (2012). Ultra magnetic liposomes for MR imaging, targeting, and hyperthermia. *Langmuir*, *28*(32), 11843–11851.

Belloni, M., Uberti, D., Rizzini, C., Jiricny, J., & Memo, M. (1999). Induction of two DNA mismatch repair proteins, MSH2 and MSH6, in differentiated human neuroblastoma SH-SY5Y cells exposed to doxorubicin. *Journal of Neurochemistry*, *72*(3), 974–979.

Bolisetty, S., Vallooran, J. J., Adamcik, J., & Mezzenga, R. (2013). Magnetic-responsive hybrids of Fe_3O_4 Nanoparticles with β-lactoglobulin amyloid fibrils and nanoclusters. *ACS Nano*, *7*(7), 6146–6155.

Casula, M. F., Floris, P., Innocenti, C., Lascialfari, A., Marinone, M., Corti, M., et al. (2010). Magnetic resonance imaging contrast agents based on iron oxide superparamagnetic ferrofluids. *Chemistry of Materials*, *22*(5), 1739–1748.

Chang, R. L. S., Crawford, M. P., & West, M. D. (1980). An assessment of the potential use of anionic dextrans as a plasma substitute. *Journal of Biomedical Engineering*, *2*(1), 41–44.

Chen, W., Huang, Q., Ou, W., Hao, Y., Wang, L., Zeng, K., et al. (2014). Self-reporting liposomes for intracellular drug release. *Small*, *10*(7), 1261–1265.

Gomes, J., Rank, A., Kronenberger, A., Fritz, J., Winterhalter, M., & Ramaye, Y. (2009). Polyelectrolyte-coated unilamellar nanometer-sized magnetic liposomes. *Langmuir*, *25*(12), 6793–6799.

Goren, D., Horowitz, A. T., Tzemach, D., Tarshish, M., Zalipsky, S., & Gabizon, A. (2000). Nuclear delivery of doxorubicin via folate-targeted liposomes with bypass of multidrug-resistance efflux pump. *Clinical Cancer Research*, *6*(5), 1949–1957.

Hao, R., Yu, J., Ge, Z. G., Zhao, L. Y., Sheng, F. G., Xu, L. L., et al. (2013). Developing Fe_3O_4 nanoparticles into an efficient multimodality imaging and therapeutic probe. *Nanoscale*, *5*(23), 11954–11963.

Huang, B. R., Chen, P. Y., Huang, C. Y., Jung, S. M., Ma, Y. H., Wu, T., et al. (2009). Bioavailability of magnetic nanoparticles to the brain. *Journal of Magnetism and Magnetic Materials*, *321*(10), 1604–1609.

Ishida, T., Harada, M., Wang, X. Y., Ichihara, M., Irimura, K., & Kiwada, H. (2005). Accelerated blood clearance of PEGylated liposomes following preceding liposome injection: Effects of lipid dose and PEG surface-density and chain length of the first-dose liposomes. *Journal of Controlled Release*, *105*(3), 305–317.

Jordan, A., Scholz, R., Wust, P., Fahling, H., & Felix, R. (1999). Magnetic fluid hyperthermia (MFH): Cancer treatment with AC magnetic field induced excitation of biocompatible superparamagnetic nanoparticles. *Journal of Magnetism and Magnetic Materials*, *201*, 413–419.

Katagiri, K., Imai, Y., Koumoto, K., Kaiden, T., Kono, K., & Aoshima, S. (2011). Magnetoresponsive on-demand release of hybrid liposomes formed from Fe_3O_4 nanoparticles and thermosensitive block copolymers. *Small*, *7*(12), 1683–1689.

Kitaoka, M., & Robyt, J. F. (1999). Mechanism of the action of *Leuconostoc mesenteroides* B-512FMC dextransucrase: Kinetics of the transfer of D-glucose to maltose and the effects of enzyme and substrate concentrations. *Carbohydrate Research*, *320*(3–4), 183–191.

Lahiri, J., Isaacs, L., Tien, J., & Whitesides, G. M. (1999). A strategy for the generation of surfaces presenting ligands for studies of binding based on an active ester as a common reactive intermediate: A surface plasmon resonance study. *Analytical Chemistry*, *71*(4), 777–790.

Lai, S. M., Hsiao, J. K., Yu, H. P., Lu, C. W., Huang, C. C., Shieh, M. J., et al. (2012). Polyethylene glycol-based biocompatible and highly stable superparamagnetic iron oxide nanoclusters for magnetic resonance imaging. *Journal of Materials Chemistry B*, *22*(30), 15160–15167.

Lawaczeck, R., Bauer, H., Frenzel, T., Hasegawa, M., Ito, Y., Kito, K., et al. (1997). Magnetic iron oxide particles coated with carboxydextran for parenteral administration and liver contrasting. Pre-clinical profile of SH U555A. *Acta Radiologica*, *38*, 584–597.

Liao, Z. Y., Wang, H. J., Lv, R. C., Zhao, P. Q., Sun, X. Z., Wang, S., Su, W. Y., Niu, R. F., & Chang, J. (2011). Polymeric liposomes-coated superparamagnetic iron oxide nanoparticles as contrast agent for targeted magnetic resonance imaging of cancer cells. *Langmuir*, *27*(6), 3100–3105.

Lunov, O., Syrovets, T., Buchele, B., Jiang, X. E., Rocker, C., Tron, K., et al. (2010). The effect of carboxydextran-coated superparamagnetic iron oxide nanoparticles on c-Jun N-terminal kinase-mediated apoptosis in human macrophages. *Biomaterials*, *31*(19), 5063–5071.

Mailander, V., Lorenz, M. R., Holzapfel, V., Musyanovych, A., Fuchs, K., Wiesneth, M., Walther, P., Landfester, K., & Schrezenmeier, H. (2008). Carboxylated superparamagnetic iron oxide particles label cells intracellularly without transfection agents. *Molecular Imaging and Biology*, *10*(3), 138–146.

Martina, M. S., Fortin, J. P., Menager, C., Clement, O., Barratt, G., Grabielle-Madelmont, C., et al. (2005). Generation of superparamagnetic liposomes revealed as highly efficient MRI contrast agents for in vivo imaging. *Journal of the American Chemical Society*, *127*(30), 10676–10685.

Massart, R. (1981). Preparation of aqueous magnetic liquids in alkaline and acidic media. *IEEE Transactions on Magnetics*, *MAG-17*(2), 1247–1248.

Mikhaylov, G., Mikac, U., Magaeva, A. A., Itin, V. I., Naiden, E. P., Psakhye, I., et al. (2011). Ferri-liposomes as an MRI-visible drug-delivery system for targeting tumours and their microenvironment. *Nature Nanotechnology*, *6*(9), 594–602.

Mura, S., & Couvreur, P. (2012). Nanotheranostics for personalized medicine. *Advanced Drug Delivery Reviews*, *64*(13), 1394–1416.

Nair, M., Guduru, R., Liang, P., Hong, J. M., Sagar, V., & Khizroev, S. (2013). Externally controlled on-demand release of anti-HIV drug using magneto-electric nanoparticles as carriers. *Nature Communications*, *4*, 1707.

Nappini, S., Al Kayal, T., Berti, D., Norden, B., & Baglioni, P. (2011). Magnetically triggered release from giant unilamellar vesicles: Visualization by means of confocal microscopy. *Journal of Physical Chemistry Letters*, *2*(7), 713–718.

Nappini, S., Bombelli, F. B., Bonini, M., Norden, B., & Baglioni, P. (2010). Magnetoliposomes for controlled drug release in the presence of low-frequency magnetic field. *Soft Matter*, *6*(1), 154–162.

Ning, S., Huang, Q., Sun, X., Li, C., Zhang, Y., Li, J., et al. (2011). Carboxymethyl dextran-coated liposomes: Toward a robust drug delivery platform. *Soft Matter*, *7*(19), 9394–9401.

Pain, D., Das, P. K., Ghosh, P., & Bachhawat, B. K. (1984). Increased circulatory half-life of liposomes after conjunction with dextran. *Journal of Biosciences*, *6*, 811–816.

Pothayee, N., Balasubramaniam, S., Jain, N., Hu, N., Lin, Y. N. A., Davis, R. M., et al. (2013). Magnetic nanoclusters with hydrophilic spacing for dual drug delivery and sensitive magnetic resonance imaging. *Journal of Materials Chemistry B*, *1*(8), 1142–1149.

Pradhan, P., Giri, J., Rieken, F., Koch, C., Mykhaylyk, O., Doblinger, M., et al. (2010). Targeted temperature sensitive magnetic liposomes for thermo-chemotherapy. *Journal of Controlled Release*, *142*(1), 108–121.

Preiss, M. R., & Bothun, G. D. (2011). Stimuli-responsive liposome-nanoparticle assemblies. *Expert Opinion on Drug Delivery*, *8*(8), 1025–1040.

Reches, M., & Gazit, E. (2006). Controlled patterning of aligned self-assembled peptide nanotubes. *Nature Nanotechnology*, *1*(3), 195–200.

Sanson, C., Diou, O., Thevenot, J., Ibarboure, E., Soum, A., Brulet, A., et al. (2011). Doxorubicin loaded magnetic polymersomes: Theranostic nanocarriers for MR imaging and magneto-chemotherapy. *ACS Nano*, *5*(2), 1122–1140.

Shiraishi, K., & Yokoyama, M. (2013). Polymeric micelles possessing polyethyleneglycol as outer shell and their unique behaviors in accelerated blood clearance phenomenon. *Biological & Pharmaceutical Bulletin*, *36*(6), 878–882.

Smistad, G., Boyum, S., Alund, S. J., Samuelsen, A. B. C., & Hiorth, M. (2012). The potential of pectin as a stabilizer for liposomal drug delivery systems. *Carbohydrate Polymers*, *90*(3), 1337–1344.

Soenen, S. J., Vande Velde, G., Ketkar-Atre, A., Himmelreich, U., & De Cuyper, M. (2011). Magnetoliposomes as magnetic resonance imaging contrast agents. *Wiley Interdisciplinary Reviews—Nanomedicine and Nanobiotechnology*, *3*(2), 197–211.

Spera, R., Petralito, S., Liberti, M., Merla, C., d'Inzeo, G., Pinto, R., et al. (2014). Controlled release from magnetoliposomes aqueous suspensions exposed to a low intensity magnetic field. *Bioelectromagnetics*, *35*(4), 309–312.

Sugahara, S., Kajiki, M., Kuriyama, H., & Kobayashi, T. R. (2007). Complete regression of xenografted human carcinomas by a paclitaxel-carboxymethyl dextran conjugate (AZ10992). *Journal of Controlled Release*, *117*(1), 40–50.

Tai, L. A., Tsai, P. J., Wang, Y. C., Wang, Y. J., Lo, L. W., & Yang, C. S. (2009). Thermosensitive liposomes entrapping iron oxide nanoparticles for controllable drug release. *Nanotechnology*, *20*(13), 135101.

Teschke, O., & de Souza, E. F. (2002). Liposome structure imaging by atomic force microscopy: Verification of improved liposome stability during adsorption of multiple aggregated vesicles. *Langmuir*, *18*(17), 6513–6520.

Thorek, D. L. J., & Tsourkas, A. (2008). Size, charge and concentration dependent uptake of iron oxide particles by non-phagocytic cells. *Biomaterials*, *29*(26), 3583–3590.

Wang, B., Chen, K. F., Yang, R. D., Yang, F., & Liu, J. (2014). Stimulus-responsive polymeric micelles for the light-triggered release of drugs. *Carbohydrate Polymers*, *103*, 510–519.

Xiong, X. B., Huang, Y., Lu, W. L., Zhang, X., Zhang, H., Nagai, T., et al. (2005). Enhanced intracellular delivery and improved antitumor efficacy of doxorubicin by sterically stabilized liposomes modified with a synthetic RGD mimetic. *Journal of Controlled Release*, *107*(2), 262–275.